

A.J. Jiao · R. Riegler · H.B. Ma · G. P. Peterson

## Thin film evaporation effect on heat transport capability in a grooved heat pipe

Received: 5 August 2004 / Accepted: 21 October 2004 / Published online: 23 February 2005  
© Springer-Verlag 2005

**Abstract** A theoretical model predicting the heat transfer performance occurring in a grooved heat pipe is developed. The model includes the effects of groove geometry, thin film evaporation, contact angle, and film condensation. The numerical results show that the groove geometry significantly affects the thin film evaporation and condensation. The thin film evaporation plays a key role in the total effective thermal conductivity and determines a limit for the maximum amount of heat transport through the micro regions for a given evaporator geometry. While the contact angle can influence the capillary limitation, it significantly affects the thin film evaporation and the total effective thermal conductivity of a groove heat pipe. In order to verify the theoretical analysis, an experimental investigation on a grooved heat pipe was conducted. The current investigation will result in a better understanding of thin film evaporation and its effect on the maximum heat transport in a grooved heat pipe.

**Keywords** Heat pipe · Thin film heat transfer · Condenser · Evaporator

### List of symbols

$A$	Section area
$a$	Constant
$b$	Constant
$D_{h, l}$	Liquid flow hydraulic diameter (m)
$f$	Friction coefficient
$h_{fg}$	Latent heat of vaporization (J/kg)
$h_t$	Height of groove wall (m)
$h_y$	Height of liquid flow along the $y$ axis (m)

$K$	Constant in Eq. 6
$k$	Conductivity (W/m K)
$L$	Length (m)
$m$	Mass of charged working fluid (g)
$N$	Number of grooves
$P_v$	Perimeter of the vapor space
$p$	Pressure (N/m <sup>2</sup> )
$Q$	Heat transfer load (W)
$q$	Heat flux (W/m <sup>2</sup> )
$R$	Gas constant (J/kg K)
$Re$	Reynolds Number
$R_{in}$	Interior radius of heat pipe (m)
$r$	Radius (m)
$s$	Coordinate (m)
$T$	Temperature (K)
$u$	Velocity (m/s)
$\bar{u}$	Average velocity (m/s)
$W$	Width of groove (m)
$x$	Coordinate (m)
$y$	Coordinate (m)
$z$	Coordinate (m)
$\alpha$	Contact angle (°)
$\beta$	Angle defined in Fig. 1 (°)
$\phi$	Tilt angle (°)
$\delta$	Film thickness (m)
$\delta_0$	Non-evaporating film thickness (m)
$\eta$	Coordinate (m)
$\mu$	Viscosity (N·s/m <sup>2</sup> )
$\theta$	Angle defined in Fig. 1 (°)
$\rho$	Density (kg/m <sup>3</sup> )
$\sigma$	Surface tension (N/m)

A.J. Jiao · R. Riegler · H.B. Ma (✉)  
Department of Mechanical and Aerospace Engineering,  
University of Missouri, Columbia, MO 65211, USA  
E-mail: mah@missouri.edu  
Tel.: +1-573-8845944

G. P. Peterson  
Rensselaer Polytechnic Institute,  
Troy, NY 12180, USA

### Subscripts

$a$	Adiabatic
$c$	Condenser
$e$	Vapor, evaporator
$eff$	Effective
$h, v$	Vapor hydraulic
$l$	Liquid

<i>mic</i>	Micro region
<i>mac</i>	Macro region
<i>sat</i>	Saturated
<i>tot</i>	Total
<i>v</i>	Vapor
<i>w</i>	Wall
<i>z</i>	<i>z</i> coordinate
$\delta$	Thickness
$\delta, v$	Liquid–vapor interface

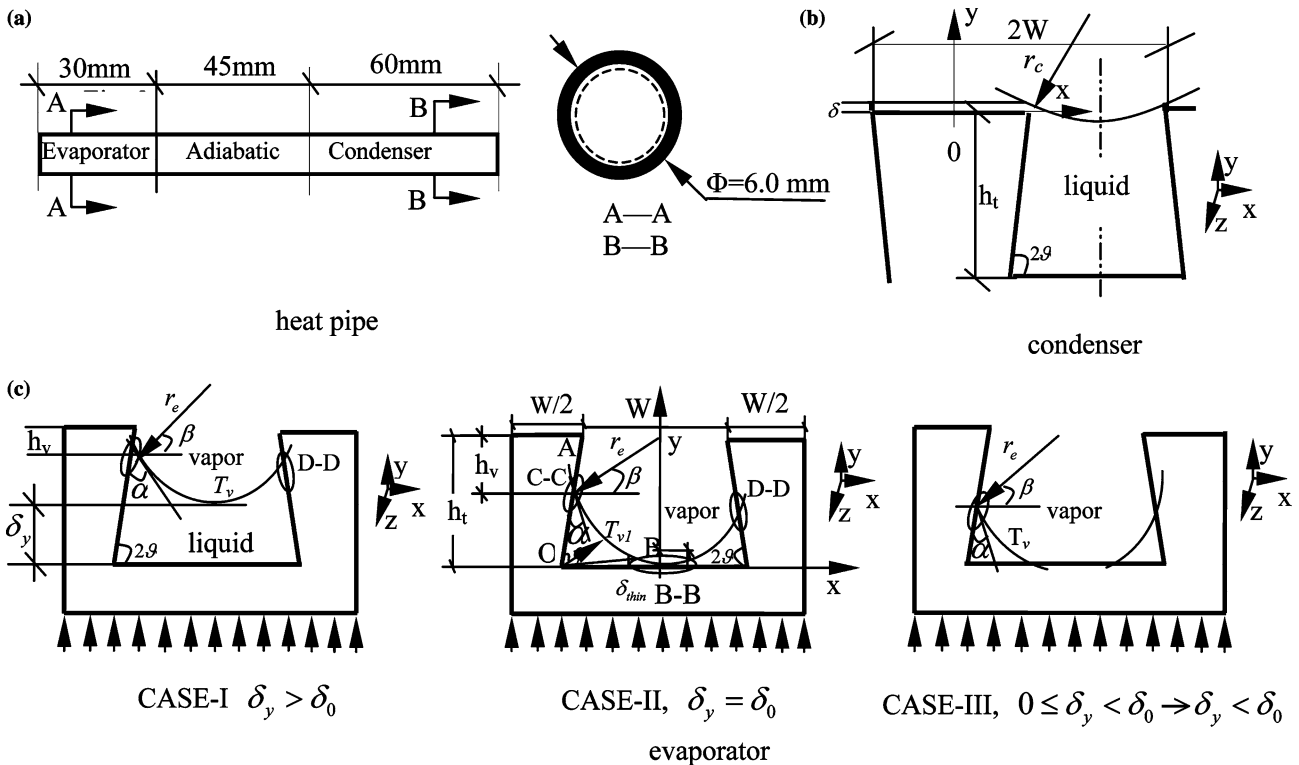
**1 Introduction**

Micro/minature heat pipes have been widely used in many electronic systems because of their high heat transport capacity and high level of uniform temperature distribution. In the design of heat pipes, a number of heat transfer limitations (Ma and Peterson 1996; Hopkins et al. 1999) should be taken into consideration. These limitations determine the maximum heat transport occurring in a heat pipe. Most of the previous investigations focus on the capillary heat transport capability because the fundamental phenomena that govern the operation of micro heat pipes arises from the

difference in the capillary pressure across the liquid–vapor interfaces in the evaporator and condenser regions. Several theoretical models and experimental investigations of the capillary heat transport limitations on those micro/minature heat pipes have been completed by Ha and Peterson (1994), Ma and Peterson (1996), Hopkins et al. (1999), and Babin and et al. (1990). These investigations are useful for understanding the heat transport mechanisms occurring in the micro/minature heat pipe.

With the development of micro-electronics and micro manufacturing technologies, the computational speed of the operating systems creates very highly concentrated levels of heat flux. The dissipation of these high heat fluxes presents unique challenges for heat removal. Therefore, it is necessary to further increase the effective thermal conductivity of a heat pipe in order to meet these new requirements. While conventional heat transport limitations govern the heat transport capability, the effective thermal conductivity, i.e., the relationship between the temperature difference and the input heat power, must also be investigated. Several theoretical models (Demsy and Ma 2004; Ma and Peterson 1997; Stephan and Busse 1993; Wayner et al. 1976) capable of predicting the effects of the thin film region on the evaporating heat transfer have been developed, particularly for trapezoidal-grooved heat pipes, in order to determine the maximum evaporating heat transfer through the thin film region (Ma and Jiao 2004). In the current investigation, the momentum conservation and Laplace–Young equations were used to develop a mathematical

**Fig. 1** Schematic of the heat pipe used in the theoretical model and experimental investigation. (a) Heat pipe. (b) Condenser. (c) Evaporator



model to predict the temperature drops in the condenser and evaporator for a trapezoidal-grooved heat pipe. The predicted temperature drop was then compared with the experimental results. The results from the numerical model showed good agreement with the experimental data.

## 2 Theoretical analysis

Figure 1a illustrates the schematic of the heat pipe employed in the theoretical model and experimental investigation. Figure 1b shows the configuration of the capillary grooves, the liquid flow, and the film condensation in the condenser. Figure 1c presents the liquid flow profiles and thin film region distributions in the evaporator under different heat loads. Ma and Jiao (2004) developed a model to predict the contact angle effect on the thin film profile, the heat flux distribution, and the ratio of  $Q_{mic}/Q_{tot}$  versus  $T_w - T_e$ . In the model, Ma and Jiao (2004) mainly focused on CASE II, where  $\delta_y = \delta_0$ , and their theoretical predictions indicated that the thin film heat transfer plays a key role in the evaporation. For CASE III ( $0 \leq \delta_y < \delta_0$ ), the thin film heat transfer is divided into two triangle-shaped areas. Thin film heat transfer for the triangular-grooved heat pipe has been studied by a number of investigators (Ma and Peterson 1996; Peterson and Ma 1996, 1999; Ha and Peterson 1994). CASE I can be considered as  $\delta_0 \leq \delta_y \leq h_t$  and the heat transfer characteristics in this case should be paid more attention. Therefore, this paper will mainly focus on the investigation of CASE I.

### 2.1 Capillary flow

In order to determine the temperature drops in the evaporator and condenser, the meniscus radius variation from the evaporator to the condenser must first be determined. For a heat pipe operating in a steady state, a given heat transport will determine the meniscus radius variation from the cap end of the evaporator section to the radius in the condenser section. To simplify the calculation, the average radii at the evaporator and condenser are considered. In order to pump the condensate back to the evaporating section for a given heat input, the capillary pressure must be equal to the summation of the total pressure drops, i.e.

$$\sigma \left( \frac{1}{r_e} - \frac{1}{r_c} \right) = \left[ \frac{4f_l Re \mu_l}{2D_{h,l}^2} \times \frac{Q_{tot}}{N \rho_l A_{ac} h_{fg}} + \left( \frac{f_v Re_{h,v} \mu_v}{2r_{h,v}^2 A_v \rho_v h_{fg}} \right) Q_{tot} - \rho_l g \sin \phi \right] L_{eff} \quad (1)$$

where:

$$\begin{aligned} L_{eff} &= \frac{L_c}{2} + L_a + \frac{L_e}{2} \\ \beta &= \alpha + 2\vartheta - \frac{\pi}{2} \\ r_{h,v} &= \frac{4A_v}{P_v} \\ A_v &= \pi R_{in}^2 + A_{ac} - A_{ae} \\ P_v &= \pi R_{in} + N \left[ 2r_e \left( \frac{\pi}{2} - \beta \right) + \frac{h_t}{\sin 2\vartheta} \right] \\ h_v &= h_t - [\delta_y + r_e(1 - \sin \beta)] \end{aligned} \quad (2)$$

Since the cross-sectional area of the liquid flow in the condenser is different from that occurring in the evaporator,  $A_{ac}$  and  $D_{h,l}$  for one groove channel in the condenser can be written as

$$\begin{aligned} A_{ac} &= h_t(W + h_t ctg 2\vartheta) \\ D_{h,l} &= \frac{A_{ac}}{\left( \frac{h_t}{\sin 2\vartheta} + W + h_t ctg 2\vartheta \right)} \end{aligned} \quad (3)$$

For the evaporator, the cross-sectional area of the liquid fluid flow for one groove channel can be expressed as

$$\begin{aligned} A_{ae} &= (h_t - h_v)[W + 2r_e \cos \beta + 2(h_t - h_v) ctg 2\vartheta] \\ &\quad - r_e^2 \left( \frac{\pi}{2} - \beta - \cos \beta \sin \beta \right) \end{aligned} \quad (4)$$

and it should be noted that, for a given heat transport load, the meniscus radius in the evaporator is given. Using the following expression

$$r_e = \frac{W/2 + (h_t - \delta_y) ctg 2\vartheta}{\cos \beta + (1 - \sin \beta) ctg 2\vartheta} \quad (5)$$

$\delta_y$  is determined for a given heat transfer load. For the condensate flow in an open trapezoidal groove, the results by Kim et al. (2003) can be used as follows

$$\begin{aligned} f_l Re &= 14.11 \alpha^{0.06009} \\ &\quad \times \exp \left\{ -0.5 \times \left[ \frac{\log(K/22.22 \alpha^{-0.3366})}{(2.083 \alpha^{0.0372})} \right]^2 \right\} \end{aligned} \quad (6)$$

where  $K = h_t / (W + 2h_t ctg 2\vartheta)$ .

### 2.2 Heat transfer in the condenser

As shown in Fig. 1(b), the pressure gradient in the condensate film can be calculated as

$$\frac{dP_{l\delta}}{dx} = \frac{4f \cdot \frac{1}{2} \rho \bar{u}_\delta^2}{\delta} = \frac{4f Re_\delta \mu \bar{u}_\delta}{2\delta^2} \quad (7)$$

where

$$Re_\delta = \frac{\delta \rho \bar{u}_\delta}{\mu}, \text{ and } \bar{u}_\delta L_c \delta \rho_l = m_s = \frac{q_s}{h_{fg}} = \frac{Q_{mic}}{N h_{fg}} \quad (8)$$

Substituting Eq. 8 into Eq. 7 and integrating Eq. 7, the pressure drop can be determined, and this value is equal to the capillary pumping pressure, i.e.

$$\Delta P_{l\delta} = \int_0^{\frac{W}{2}} \frac{2f Re_\delta \mu}{\delta^3} \frac{q_s}{L_c \rho h_{fg}} dx = \frac{f Re_\delta \mu W Q_{mic}}{N \delta^3 L_c \rho h_{fg}} = \frac{\sigma}{r_c} \quad (9)$$

where  $fRe_\delta = 6$  and  $r_e$  can be determined from Eq. 1 for a given heat transport. The thin film thickness can be calculated by Eq. 9. Therefore, the heat transfer  $Q_{mic}$  through the condensate thin film can be determined as

$$Q_{mic} = 2N \int_0^{lc} \int_0^{\frac{\pi}{2}} k \frac{T_w - T_{\delta,v}}{\delta} dx dz \quad (10)$$

Combining the heat transport from the macro region, the temperature drop in the condenser can be obtained.

### 2.3 Thin film heat transfer in the evaporator

Figure 2 illustrates the thin film distribution for CASE I in the evaporator. The meniscus radius shown in Eq. 5 depends on the groove configuration, contact angle, and heat load. For a given grooved heat pipe investigated here, the groove configuration parameters are known and the total amount of charged working fluid is given, the meniscus radius and  $\delta_y$  will be only dependent on the heat load, which can be determined by Eqs. 1 and 5.

Heat transport through the thin film region plays an important role in micro/miniature heat pipes and it is reasonable to consider the heat transfer through this region as one-dimensional heat conduction. Based on this assumption and the groove configuration parameters, as shown in Fig. 1(c), heat transfer through this thin film region can be calculated as

$$\begin{aligned} Q_{mic} &= 2N \int_0^{l_s} k_l \frac{T_w - T_{\delta,v}}{\delta_\eta} L_e ds \\ &= -N \int_{r_e[1+\cos(2\vartheta+\alpha)]+\delta_y}^y k_l \frac{T_w - T_{\delta,v}}{\delta_\eta \sin 2\vartheta} L_e dy \end{aligned} \quad (11)$$

where

$$\delta_\eta = \frac{W}{2} + ctg 2\vartheta (h_t - y) - \sqrt{r_e^2 - [y - (r_e - \delta_y)]^2} \quad (12)$$

$$\begin{aligned} y &= r_e(1 - \sin \beta) + \delta_y \\ \text{and } \delta_y &\leq y \leq r_e[1 - \sin \beta] + \delta_y \\ \delta_y &= \delta_0, r_0 \rightarrow \infty, T_{\delta,v} = T_w; \text{ at } s = 0 \\ \delta_0 &= \exp\left\{ \left[ \frac{T_w}{T_v} - 1 \right] \left( \frac{h_{fg}}{RT_w} \right) - \ln a \right\} / b \end{aligned} \quad (13)$$

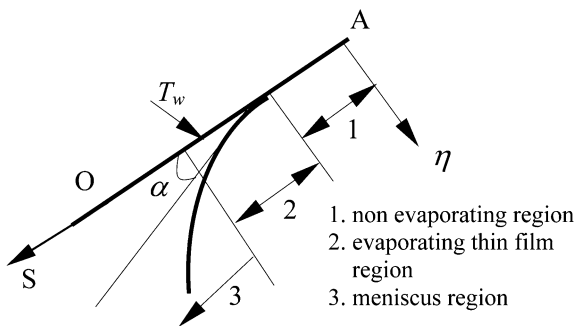


Fig. 2 Thin film profile along the A–O direction

It should be noted that the disjoining pressure for thin film evaporation and its effect on the interface thermal resistance are included.

### 2.4 Heat transfer through the macro region

Because the groove as shown in Fig. 1 is very small and the Bond number is much less than 1, the temperature distribution in the macro liquid film region can be described by the two-dimensional, steady-state heat conduction equation, i.e.

$$\frac{\partial^2 T}{\partial x^2} + \frac{\partial^2 T}{\partial y^2} = 0 \quad (14)$$

Although the geometry is not regular, the solution for Eq. 14 can be readily obtained using commercial software (FLUENT), and the heat transfer through the macro region can be obtained. The total heat transfer can be expressed as

$$Q_{tot} = Q_{mic} + Q_{mac} \quad (15)$$

It is reasonable to neglect the heat transfer through the macro region in the condenser, but the heat transfer through the macro region in the evaporator should be considered. The ratio of the heat transport through the micro thin film region and the macro region has been calculated by Ma and Jiao (2004).

## 3 Experimental system

The experimental system shown in Fig. 3 was used to evaluate the heat pipe and verify the mathematical model. The system consisted of a heat pipe, constant temperature circulator, power supply and measurement unit, and data acquisition system. The heat pipe was nestled within a cooling reservoir at one end and inserted into a heating device at the other. The evaporator end of the heat pipe was encased in a heater and surrounded in insulation. The heater was attached to a power supply for the source and a bench-top multi-meter was used to measure the resistance and the

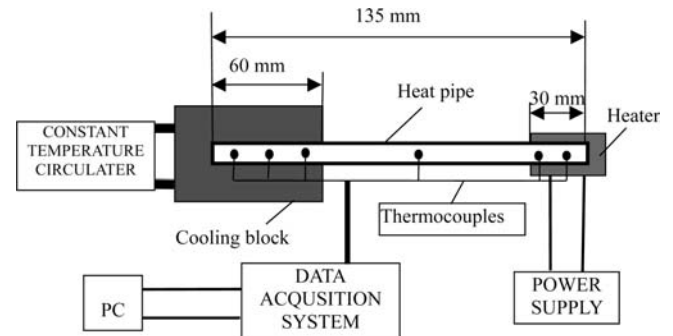


Fig. 3 Schematic of the experimental system

voltage input from the power supply. The condensing end of the heat pipe was enclosed in the cooling reservoir that was maintained at a constant temperature ( $60.0 \pm 0.2^\circ\text{C}$ ) by a cooling bath. The adiabatic section of the heat pipe was comprised of the space between the end of the heater and the beginning of the cooling chamber. A series of thermocouples were attached to the heat pipe, which led to an IO/Tech Personal DAQ56 data acquisition system controlled by a personal computer. The most important results of the experiment were the resulting temperature differences between the evaporator and the condenser

$$\Delta T = \left( \frac{T_{e,1} + T_{e,2} + T_{e,3}}{3} \right) - \left( \frac{T_{c,1} + T_{c,2}}{2} \right) \quad (16)$$

where  $T_{e,1}$ ,  $T_{e,2}$ , and  $T_{e,3}$  represent the thermocouple measurements in the evaporator and  $T_{c,1}$  and  $T_{c,2}$  represent the measurements in the condenser.

### 4 Results and discussion

In addition to the heat pipe configuration shown in Fig. 1, the detailed dimensions of the grooves are:  $2W = 0.000262$  m,  $h_t = 0.000195$  m,  $L_e = 0.06$  m,  $L_a = 0.045$  m,  $L_c = 0.03$  m,  $m = 0.508$  g,  $2\vartheta = 75.8^\circ$ ,  $R_{in} = 0.0025$  m, and the groove number = 60, were used in the current model with the thermophysical properties of copper and pure saturated water at  $60^\circ\text{C}$ .

Figure 4 illustrates the heat load effect on the meniscus radius under different contact angles in the evaporator. As shown, the meniscus radius increases with increases in the heat load. As the radius,  $r_e$ , and the thickness,  $\delta_y$ , are determined by the heat load using Eqs. 1 and 5; the liquid flow profile and temperature drop can be obtained for a given contact angle and heat load. As shown in Fig. 5, the temperature drop is different at the same heat load, depending on the contact

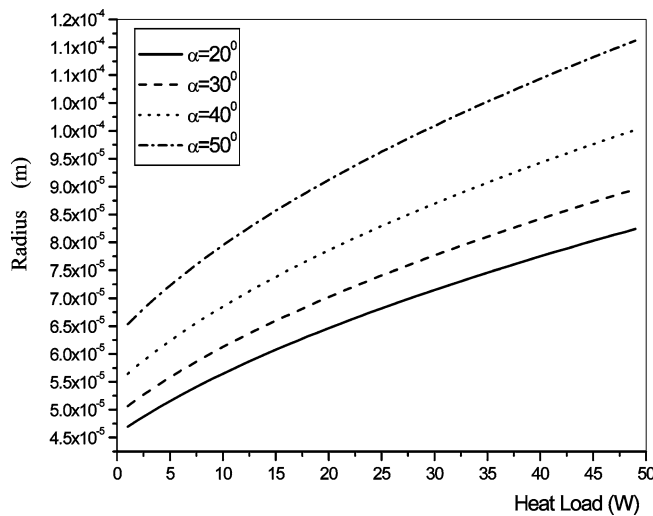


Fig. 4 Contact angle effect on the meniscus radius

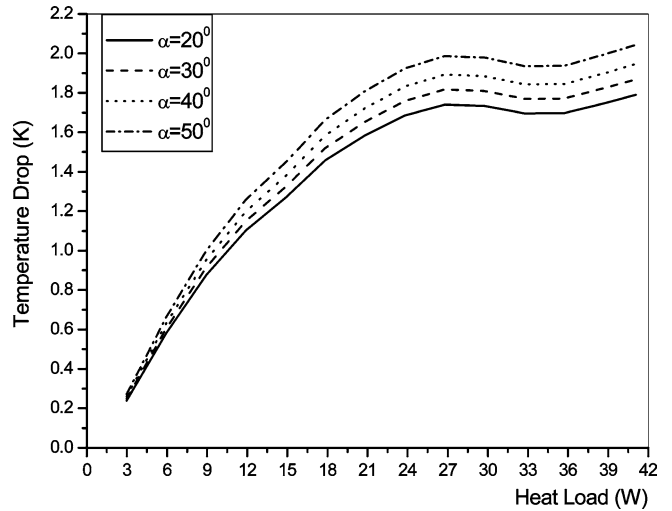


Fig. 5 Contact angle effect on the temperature drop in the evaporator

angle. The meniscus radius decreases with a decreasing contact angle and directly increases the capillary pumping ability and heat transport capability. More importantly, as the contact angle decreases, the thin film region is enlarged and effectively enhances the heat transport capability, resulting in a smaller temperature drop in the evaporator for the same heat load, as shown in Fig. 5.

Figure 6 shows the temperature distribution in the macro region of the liquid film in the groove at  $\alpha = 40^\circ$  and  $Q_{in} = 35W$ . The temperature difference between the wall and the vapor flow is equal to 1.8 K and the temperature difference between two isotherms is equal to 0.09 K. These results were obtained using the FLUENT software.

As shown in Fig. 7, the temperature drop in the condenser varies nonlinearly at a low heat load, but nearly linearly as the heat load increases. The temperature drop in the evaporator, as shown in Figs. 5

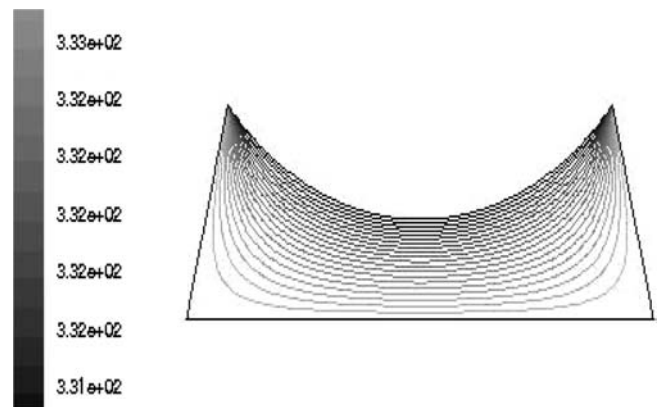


Fig. 6 Temperature distribution in the bulk liquid region in the evaporator ( $\alpha = 40^\circ$  and  $Q_{in} = 35W$ , the temperature difference between two isotherms is 0.09 K)

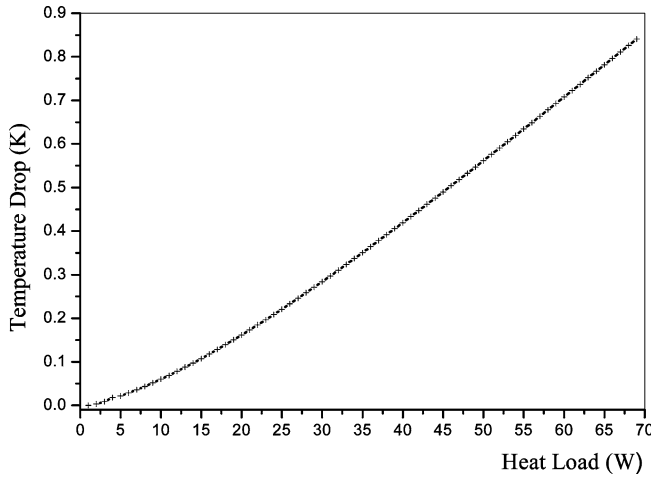


Fig. 7 Temperature drop in the condenser

and 7, plays a much more important role than in the condenser. For example, as  $Q_{\text{tot}} = 18\text{ W}$ ,  $\Delta T_c = 1.52\text{ K}$  at  $\alpha = 30^\circ$  in the evaporator and  $\Delta T_c = 0.14\text{ K}$  in the condenser, respectively. The temperature drop in the evaporator is much larger than that in the condenser for the same heat load. One reason is that the condenser length is twice the evaporator length and the thin film region in the condenser is much larger than that in the evaporator.

As shown in Fig. 8, the numerical results predicted by the theoretical model have been compared with the experimental results. In the low heat load region, the numerical results are in good agreement with the experimental results. However, as the heat load increases, the theoretical results deviate from the experimental results. The experimental results show a step function increase as the heat load approaches  $26\text{ W}$ , while the respective jump in the theoretical results occurs as the heat load reaches  $33\text{ W}$ . The main reason for this is that  $\delta_y$  becomes smaller and the liquid film becomes thinner as the heat load increases. When the heat load is large enough and  $\delta_y = \delta_0$ , the heat transfer has been dramatically enhanced. As a result, the temperature drop does not increase, but rather, decreases as the heat load increases. Figure 8b shows a comparison of the thermal resistances between the theoretical prediction and the experimental results. As shown, the theoretical prediction accurately predicts the thermal resistance jump as observed in the experimental investigation. The minimum thermal resistance exists and should occur when  $\delta_y = \delta_0$ , as shown in CASE II of Fig. 1(c). If the heat load continues to increase, the thin film becomes so thin that it will rupture and separate into two triangular liquid regions, as shown in CASE III in Fig. 1(c), where the thermal resistance increases sharply. This minimum thermal resistance limitation in the design of heat pipes. Alternatively, the heat pipe can continue to function for this case, but the temperature drop increases sharply.

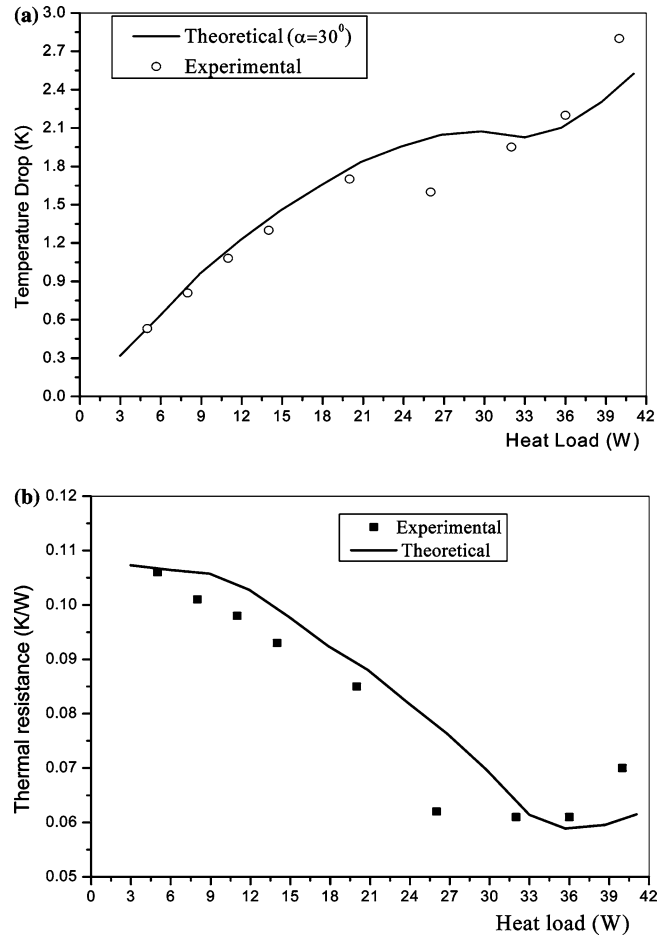


Fig. 8 Comparison of the theoretical prediction and the experimental results. (a) Temperature drop. (b) Thermal resistance

#### 4.1 Conclusions

A detailed mathematical model for predicting the thin film heat transfer characteristics in the condenser and evaporator and its effect on the temperature drop in a grooved heat pipe has been developed. The model includes the effects of the contact angle and the groove configuration on the temperature drop in the evaporator. An extensive experimental investigation has been conducted and the results have been compared with the theoretical results. The results indicate that the theoretical results predicted by the current model are in good agreement with the experimental results. For the grooved heat pipe investigated here, the temperature drop in the evaporator is much larger than in the condenser at an equivalent heat load. In order to further enhance the heat transport capability in a grooved heat pipe, it is more important to further decrease the temperature drop in the evaporator.

The results also show that, while the decrease in the contact angle decreases the meniscus radius and directly increases the capillary pumping capability and heat transport capacity, it can enlarge the thin film region and effectively enhance the heat transport capability,

resulting in a smaller temperature drop in the evaporator for the same heat load. The concept of the minimum thermal resistance limitation in the design of heat pipes has been put forward for the first time. With an increase in the heat load, the liquid flow thickness,  $\delta_y$ , becomes smaller and the liquid film thinner, and leads to a decrease in the thermal resistance of the macro liquid region. The thermal resistance will reach its minimum as  $\delta_y$  is equal to  $\delta_0$ . As the heat load continues to increase,  $\delta_y < \delta_0$  or  $\delta_y = 0$ , the liquid region will separate into two triangular liquid regions and the thermal resistance will increase sharply. The current investigation provides a better understanding of thin film evaporation and condensation, and provides a method by which the design of grooved heat pipes can be accomplished.

---

## References

- Babin BR, Peterson GP, Wu D (1990) Steady-state modeling and testing of a micro heat pipe. *J Heat Transfer* 112(3):595–601
- Demsky SM, Ma HB (2004) Thin film evaporation on a curved surface. *Microscale Thermophys Eng* 8(3):285–299
- Ha JM, Peterson GP (1994) Analytical prediction of the axial dryout point for evaporating liquids in triangular micro-grooves. *J Heat Transfer* 116(2):498–503
- Hopkins R, Faghri A, Khrustalev D (1999) Flat miniature heat pipes with micro capillary grooves. *ASME J Heat Transfer* 121(1):102–109
- Kim SJ, Seo JK, Do KH (2003) Analytical and experimental investigation on the operational characteristics and the thermal optimization of a miniature heat pipe with a grooved wick structure. *Int J Heat Mass Transfer* 46(11):2051–2063
- Ma HB, Jiao AJ (2004) Thin film evaporation on heat transport capability in a grooved heat pipe. In: *Proceedings of the 6th international symposium on heat transfer*, Beijing, China, June 2004, pp 340–345
- Ma HB, Peterson GP (1996) Experimental investigation of the maximum heat transport in triangular grooves. *J Heat Transfer* 118(3):740–746
- Ma HB, Peterson GP (1997) Temperature variation and heat transfer in triangular grooves with an evaporating film. *J Thermophys Heat Transfer* 11(1):90–97
- Peterson GP (1994) *An introduction to heat pipe*. Wiley, New York
- Peterson GP, Ma HB (1996) Theoretical analysis of the maximum heat transport in triangular grooves: a study of idealized micro heat pipes. *J Heat Transfer* 118(3):731–739
- Peterson GP, Ma HB (1999) Temperature response of heat transport in a micro heat pipe. *J Heat Transfer* 121(2):438–445
- Stephan PC, Busse CA (1993) Analysis of the heat transfer coefficient of grooved heat pipe evaporator walls. *Int J Heat Mass Transfer* 35(2):383–391
- Wayner PC Jr, Kao YK, LaCroix LV (1976) The interline heat transfer coefficient of an evaporating wetting film. *Int J Heat Mass Transfer* 19(3):487–492